Corticosteroid receptor dynamics : analysis by advanced fluorescence microscopy

Groeneweg, F.L.

Chapter 4

A combination of wide-field and TIRF single-molecule microscopy as method to visualize the membrane-associated population of the Mineralocorticoid Receptor

Femke L. Groeneweg[1], Martijn Sierksma[1,2], E. Ron de Kloet[1], John van Noort[3], Thomas Schmidt[3], Marcel J.M. Schaaf[2]

[1] Department of Medical Pharmacology, Leiden University / LUMC, Leiden, The Netherlands.
[2] Molecular Cell Biology, Institute of Biology, Leiden University, Leiden, The Netherlands.
[3] Physics of Life Processes, Institute of Physics, Leiden University, Leiden, The Netherlands.

The mineralocorticoid receptor (MR) mediates both genomic and non-genomic actions of its ligands. It is known to be localized in the cytoplasm and in the nucleus. However, over the previous decade, evidence has accumulated showing that the MR also has a smaller membrane-associated population that is involved in rapid non-genomic actions of its ligands. This membrane localization has been confirmed by electron microscopy, but the relative size of the membrane population, its regulation and its dynamics remain unknown. Total Internal Reflection Fluorescence (TIRF) microscopy is a well-established technique to image membrane proteins, since the background signal from cytoplasmic proteins is very low. Here, we utilize the combination of wide-field and TIRF single-molecule microscopy to study the dynamics of the MR near the membrane and compare this to the dynamics of the cytoplasmic population. We find that, in two different cell lines, YFP-tagged MR shows two diffusing populations, with a 30–100 fold difference in diffusion coefficients. In TIRF, a larger fraction of the imaged molecules show slow diffusion (35–51 % versus 11–30 % in wide-field microscopy). Our data suggest that this is not due to a loss of fast moving molecules in TIRF and thus represents an enriched fraction of slow-moving MRs at or near the membrane. Short-term treatment with corticosterone or membrane-impermeable corticosterone did not affect the dynamics of the MR near the membrane. In conclusion, the combination of TIRF and wide-field SMM provides a suggestion for the existence of a membrane-associated MR fraction.

4.1 Introduction

The MR is a member of the family of steroid receptors. This family encompasses a group of structurally related receptors that exert their main action within the nucleus where they bind DNA and act as transcription factors. As such they are dubbed nuclear receptors. Without hormone bound, most MRs are located in the cytoplasm while hormone binding induces nuclear translocation (Nishi et al., 2001; Sarabdjitsingh et al., 2009). In addition to its well-known nuclear function, the MR has more recently been found to mediate rapid actions of its hormones (corticosteroids and mineralocorticoids) (Grossmann et al., 2005; Karst et al., 2005, 2010; Mihailidou and Funder, 2005; Olijslagers et al., 2008; Qiu et al., 2010). These effects do not involve *de novo* transcription or protein synthesis and are therefore called non-genomic effects. Non-genomic actions are not restricted to the MR but have been found for most, if not all, steroid receptors (Hammes and Levin, 2007). Intriguingly, non-genomic effects can be induced by membrane-impermeable conjugates of the hormones and the receptors have thus been suggested to be present at the plasma membrane (Hammes and Levin, 2007; *Chapter 2*). Immunohistochemical staining with new antibodies (Gomez-Sanchez et al., 2011), cell fractionation studies (Qiu et al., 2010) and electron microscopy (Prager et al., 2010) indeed found indications for membrane localization of the MR. However, this membrane-associated fraction is postulated to be very small and does not show up with conventional microscopy. The size of this fraction, its submembrane localization and its regulation all remain unknown.

TIRF microscopy is a well-established technique for imaging of fluorescently labeled membrane-associated molecules. In TIRF microscopy, the laser is redirected so that it hits the glass-water interface between the coverglass and the specimen at a large angle relative to the optical axis. As a result, the beam is totally internally reflected, which generates an electromagnetic field, termed the evanescent field that penetrates into the specimen perpendicular to the interface. This evanescent field, is capable of exciting fluorophores present in a thin plane of 60–100 nm above the coverglass (Axelrod et al., 1983; Axelrod, 2001; Martin-Fernandez et al., 2013). TIRF microscopy thus provides images of cultured cells plated on a coverglass with a very strong enrichment for membrane-associated molecules, although membrane-associated fluorescent proteins are not exclusively excited. This technique is therefore widely used to study membrane-associated receptors, membrane-association of vesicles and near-membrane cytoskeletal dynamics (Vale et al., 1996; Sako et al., 2000; Lommerse et al., 2006; Toonen et al., 2006). In the current study, we have combined TIRF with single-molecule microscopy (SMM). In SMM, a highly sensitive CCD camera enables the imaging of single fluorophores. Time lapse imaging of single fluorophores enables an analysis of protein dynamics with very high spatial and temporal resolution (Schmidt et al., 1996; Lord et al., 2010; Persson et al., 2013). SMM can be applied using both TIRF and wide-field microscopy.

In the present study we have tested the feasibility of using TIRF microscopy to acquire images that are enriched for the membrane-associated subpopulation of (fluorescently-tagged) MR and thereby distinguish it from the cytoplasmic subpopulation. Membrane-associated molecules generally show much slower kinetics than free cytoplasmic molecules (Murase et al., 2004; Owen et al., 2009). Thus, if a sufficiently big fraction of MR exists at the membrane this should display slower protein dynamics in TIRF versus wide-field single-molecule microscopy. Indeed, we observed a larger slowly diffusing fraction of YFP-tagged MR molecules in TIRF as compared to wide-field recordings, suggesting the presence of a membrane-associated population of MR molecules. Surprisingly, short-term treatment with either corticosterone or BSA-conjugated corticosterone did not affect the kinetics of YFP-MR molecules as recorded using TIRF single-molecule microscopy.

4.2 Methods

Cell culture and DNA constructs

Generation of the expression plasmid pcDNA3.1-YFP-C10H-Ras has been described previously (Lommerse et al., 2004; Schaaf et al., 2009). YFP-MR contains the human MR gene cloned in frame into the pEFYP-C1 vector (Invitrogen), which generates an N-terminally tagged YFP-MR (described in detail in *Chapter 6*). In all experiments, either CHO (Chinese Hamster Ovary) or COS-1 cells were used. CHO cells were grown in F12 medium (GIBCO), supplemented with 10 % FBS, 0.5 % streptomycin and penicillin. COS-1 cells were grown in high glucose D-MEM (GIBCO), supplemented with 10 % FBS, 0.5 % streptomycin and penicillin. All cells were maintained at 37 °C and 5 % CO_2. One day before transfection, the cells were plated on glass coverslips (ø 13 mm) in 6-well plates, at a density of 300 000 cells per well. Glass cover slips were cleaned by sonication and 1 % RBS50 treatment and bleached by a UV-lamp to minimize (fluorescing) contaminations. The next day the cells were transfected with TransIT-CHO kit or TransIT-COS-1 kit (both Mirus) according to the manufacturer's instructions. YFP-C10H-Ras and YFP-MR were transfected at a concentration of 5 µg / 10 cm^2. Cells were incubated with the transfection mixture overnight, then washed once with PBS and placed on growth medium. 24 h before measuring, medium was replaced with serum-free medium (F-12 or D-MEM).

TIRF microscopy

For TIRF recordings we used a homebuilt microscopy setup (previously described in Koopmans et al., 2007), equipped with a 100× oil-immersion TIRF objective (NA 1.45, Nikon, Tokyo, Japan). A 100 by 100 pixel region of interest was defined at a pixel size of 213 nm. Excitation was performed using a 514 nm Arg^+ laser (Coherent, Santa Clara, CA), illuminating an area of ~600 mm^2 with a power of 1.7 µW for 12 ms. The beam was circularly polarized and displaced parallel to the optical axis of the objective, so an evanescent wave was generated by total internal reflection at the glass-water interface (Figure 4.1A). The critical angle for TIRF was checked manually (Snaar-Jagalska et al., 2013). Fluorescence light was filtered using a custom made dual-color bandpass filter (Chroma) and a long-pass filter (OG530, Schott). The

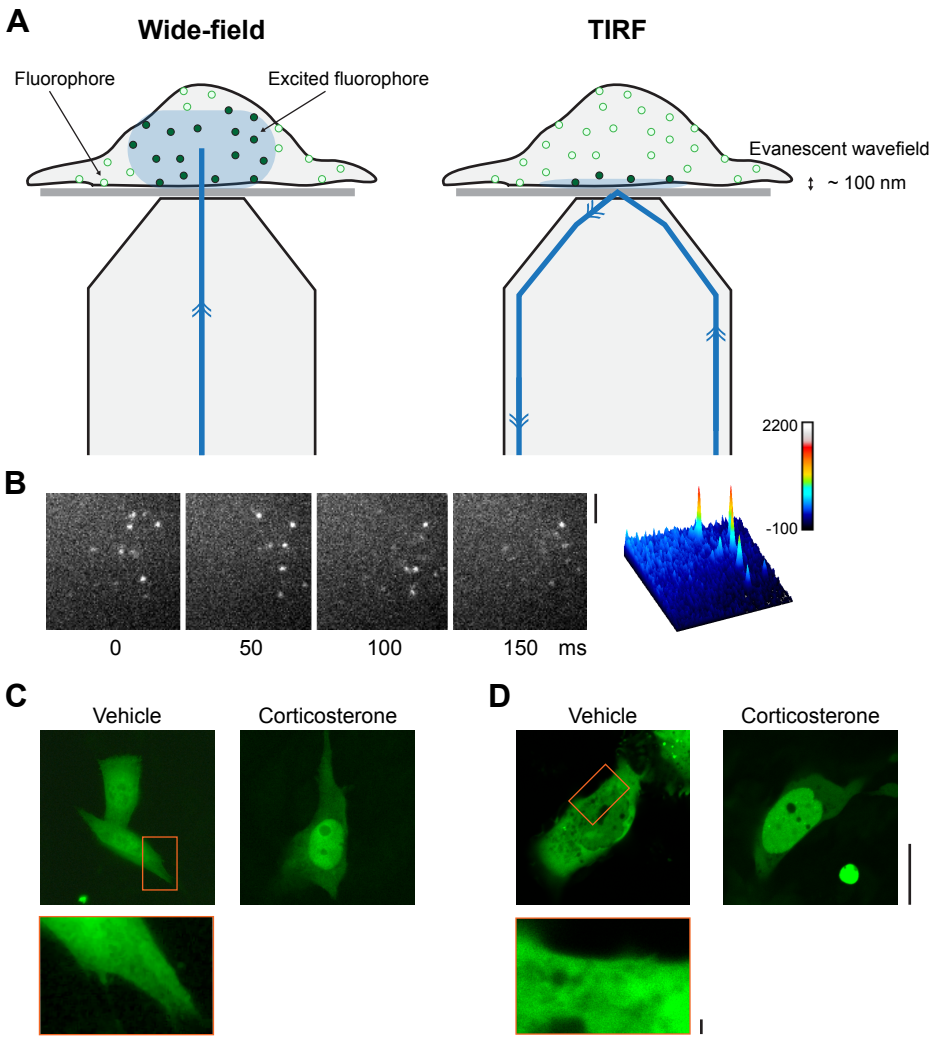

Figure 4.1: Microscopy setup
(A) Schematic diagram showing the principles of TIRF microscopy. In wide-field fluorescence microscopy the excitation light beam is directed perpendicular to the coverglass and excites fluorophores in a thick section (~1 µm). In TIRF, the excitation beam is redirected to the periphery of the objective lens and reaches the sample at a large angle relative to the optical axis. When this angle is critically large, the laser light is totally internally reflected at the glass-water interface. As a result an evanescent wave field is generated that excites fluorophores in a thin section of 60–100 nm above the coverglass. (B) Single fluorescence intensity peaks attributed to single YFP-C10H-Ras molecules are clearly discernable from the background in TIRF mode. To obtain kinetics, data sequences of 2000 images with an interval of 50 ms are obtained. (C-D) Confocal images of YFP-MR in both CHO (C) and COS-1 (D) cells. YFP-MR is seen mostly in the cytoplasm without hormone and the putative membrane-associated subpopulation is not distinguishable from the surrounding cytoplasm. After treatment with 100 nM corticosterone (16 h), YFP-MR translocates to the nucleus. *Scale bars:* 5 µm.

images were recorded by a multiplication-gain CCD camera (Cascade 512B, Roper Scientific, Trenton, NJ).

Wide-field microscopy

For wide-field recordings a customized wide-field setup (Axiovert 100TV, Zeiss) was used, equipped with a 100× / 1.4NA oil-immersion objective (Zeiss). A region-of-interest (ROI) of 50 × 50 pixels (pixel size of 220 nm) was selected. The sample was illuminated by a 514 nm argon laser at an intensity of 2 kW/cm^2 (measured at the sample). The pulse length is controlled by an acousto-optical tunable filter (AA optoelectronics, France). The YFP fluorescence signal was detected through a combination of filters (DCLP530, HQ570/80 (Chroma Technology, Brattleboro, VT) and OG530-3 (Schott, Mainz, Germany)), by a liquid-nitrogen cooled CCD camera (Princeton Instruments, Trenton, NJ). Camera read out and AOTF timing were tightly controlled.

Single-molecule imaging

For both TIRF and wide-field imaging the general procedures were identical. Transfected cells were used 2 or 3 days post transfection. For a recording, a coverslip with cells was mounted on a custom made sample-holder, the cells were washed with PBS and kept in 1 ml PBS at room temperature. Cells with moderate fluorescence intensity were selected. Cells were photobleached until single diffraction-limited spots could be distinguished. These fluorescence intensity profiles of these spots were fitted by a 3D-gaussian peak, and the center of this peak was defined as the location of the fluorescent molecule. We used a signal-to-noise ratio of > 5 and a maximal peak width of ∼600 nm as exclusion parameters.

Analysis of protein dynamics

For each cell, an image sequence of 2000 frames was recorded with a time lag of 50 ms (Figure 4.1B). We used the Particle Image Correlation Spectroscopy (PICS) method to determine the molecular mobility pattern. In PICS, the correlation between peak positions at two different time points (for example $t = 0$ ms and $t = 50$ ms) is calculated. The cumulative distribution of all distances (C_{cum}) for each time lag can be described by:

$$C_{\text{cum}}(l, \Delta t) = \frac{\left(\sum_{i=1}^{m_a} m_b(r_{ai} l)\right) \Delta t}{m_a} \tag{4.1}$$

Where r_{ai} is the position of a molecule in image A and m_a/m_b is the number of molecules in images A and B (see for further details Semrau and Schmidt, 2007). C_{cum} includes both contributions from diffusing molecules as well as distances due to random proximity to other molecules. We can then rewrite the equation as:

$$C_{\text{cum}}(l, \Delta t) = P_{\text{cum}}(l, \Delta t) + c\pi l^2 \tag{4.2}$$

In which $P_{\text{cum}}(l, \Delta t)$ is the cumulative probability function of displacement steps over the time lag, and c is the peak density. As proximity to unrelated molecules is independent of distance and solely dependent on peak density, we can fit this fraction with a straight line with offset $P_{\text{cum}}(\text{max})$ and slope of $c\pi$ and subtract it from the raw data to obtain P_{cum}. P_{cum} then includes only distances due to molecular diffusion. Population modeling is used to calculate

the diffusion pattern of the molecules. Given that the population of molecules is homogeneous, a single population of displacing molecules is determined by:

$$P_{\text{cum}}(l, \Delta t) = 1 - \exp\left(-\frac{l^2}{\text{MSD}_0(\Delta t)}\right) \tag{4.3}$$

Here MSD_0 is the mean squared displacement of one population of molecules over the time lag. However, this one fraction model did not fit the experimental data. Therefore a second fraction was introduced and the resulting equation reads as follows:

$$P_{\text{cum}}(l, \Delta t) = 1 - \left[\alpha \cdot \exp\left(-\frac{l^2}{\text{MSD}_1(\Delta t)}\right) + (1-\alpha) \cdot \exp\left(-\frac{l^2}{\text{MSD}_2(\Delta t)}\right)\right] \tag{4.4}$$

Where MSD_1 and MSD_2 denote the mean squared displacement of the first (fast) and the second (slow) fractions respectively, and α is the fraction size of the first (fast) fraction. PICS analysis was repeated for each time lag and α, MSD_1 and MSD_2 were plotted as a function of time (Δt). The data from each experimental day (on average 6.8 ± 0.7 cells/day) was pooled and analyzed together. Data is always presented as mean $\pm$ SEM. Fitting of the MSD plots was performed with SEMs as a weighting factor, and diffusion coefficients (D_{fast} and D_{slow}) were calculated using the following equation:

$$\text{MSD}(\Delta t) = 4 \cdot D \cdot \Delta t \tag{4.5}$$

Hormone treatments

For the hormone treatments, corticosterone was prediluted to a concentration of 0.1 mM in 100 % EtOH and further diluted in PBS to its final concentration of 1 mM. Corticosterone-BSA (cort-BSA) was dissolved in 0.9 % NaCl, 0.25 % carboxymethyl cellulose and 0.2 % Tween (solvent A) to 12.5 mM (1 mg/ml) and further diluted in PBS to its final concentration of 43.6 nM. There are 23 molecules of corticosterone bound to a BSA molecule, therefore the concentration of corticosterone molecules equals that of 1 µM free corticosterone. Each recorded cell was measured first without hormone (baseline) in 900 l PBS. Hereafter, the appropriate hormone (diluted in 100 ml PBS at room temperature) was added. Five minutes after the hormone was added, cells were measured again. As vehicle both 1 % EtOH and 0.4 % solvent A were used, but as the kinetics of YFP-C10H-Ras or YFP-MR was not different between the two types of vehicle solutions, they were combined for further analysis.

Statistics

In order to test for statistical significance between imaging methods we determined diffusion patterns of YFP-MR for each day of recording separately and tested significance ($n =$ number of recording days). Significance was tested with repeated measures tests, with cell type, microscopy setup or hormone treatment as between-subject factors. Statistical analysis for the peak characteristics was performed with one-way ANOVAs, with post-hoc tests according to Fisher's LSD (least significant difference) method. Statistical significance was accepted at $p < 0.05$.

4.3 Results

Single-molecule imaging using TIRF microscopy

First, as a proof-of-principle the combination of single-molecule imaging and TIRF microscopy was performed using a membrane-associated protein. For this purpose we used YFP C-terminally tagged to the membrane anchor of H-Ras, YFP-C10H-Ras. The mobility pattern of YFP-C10H-Ras has been described in previous studies (Lommerse et al., 2004; Schaaf et al., 2009). CHO cells were transiently transfected with YFP-C10H-Ras and imaged on the TIRF setup 2 to 3 days after transfection. Very low background fluorescence levels were found as well as single diffraction-limited spots(Figure 4.1B). The fluorescence intensity profiles of these spots were fitted by a 3D-gaussian peak, and peaks that could be attributed to single YFP molecules were selected using criteria based on previous studies (Harms et al., 2001).

To verify the validity of our approach, we compared the average background intensity, peak intensity, peak width and number of recorded peaks for cells transfected with YFP-C10H-Ras or YFP-tagged MR to untransfected cells. As can be seen in Figure 4.3A 8–20 fold more peaks were identified in YFP transfected cells as compared to untransfected cells. This indicates that the vast majority of selected peaks can be attributed to individual YFP molecules. In addition, higher peak intensity and peak width was obtained from peaks identified in cells transfected with either of our YFP fusion proteins (Figure 4.3B–C). We also found a larger peak width for YFP-MR transfected versus YFP-C10H-Ras transfected cells (Figure 4.3C). This larger peak width could be due to faster protein diffusion (displacement during the camera opening time) or due to a larger distance of the peak to the focus point of the objective. Both explanations could be valid, since YFP-MR generally shows faster diffusion than YFP-C10H-Ras (Table 4.1) and its partial cytoplasmic localization will also result in a larger distance to the focus point. Furthermore, more peaks per image were found for YFP-C1-H-Ras compared to YFP-MR cells. This is due to a higher percentage of molecules within the focal plane for the purely membrane localized YFP-C10H-Ras.

Series of 2000 subsequent images of these cells were obtained with time lags of $50\,\mathrm{ms}$ to investigate the dynamics of YFP-C10H-Ras. The mobility pattern of YFP-C10H-Ras was analyzed by PICS (Semrau and Schmidt, 2007). In this method, for each identified peak, the distances to all peaks in the subsequent image are recorded. This includes distances from two sources: random proximity of unrelated molecules and molecular displacements. The cumulative distribution of all distances (C_{cum}) was determined for each time lag (light grey line, Figure 4.3A). As proximity to other molecules is not dependent on distance, its contribution to C_{cum} will show a linear increase over distance (fine dotted line, Figure 4.3CA). The intercept of the fit of this linear curve represents the size of the fraction due to molecular displacements. Subtraction of this fit leaves only the distances resulting from molec-

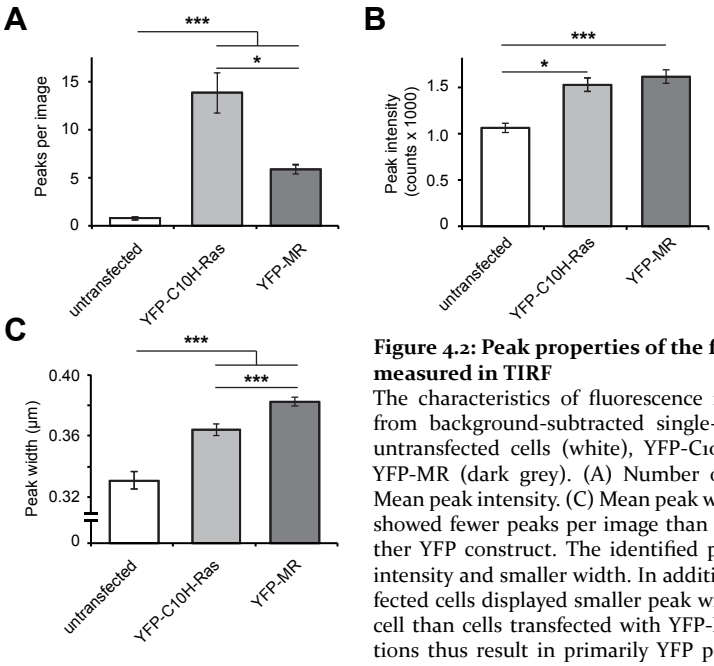

Figure 4.2: Peak properties of the fluorophores measured in TIRF
The characteristics of fluorescence intensity peaks selected from background-subtracted single-molecule recordings of untransfected cells (white), YFP-C10H-Ras (light grey) and YFP-MR (dark grey). (A) Number of peaks per image. (B) Mean peak intensity. (C) Mean peak width. Untransfected cells showed fewer peaks per image than cells transfected with either YFP construct. The identified peaks also showed lower intensity and smaller width. In addition, YFP-C10H-Ras transfected cells displayed smaller peak width and more peaks per cell than cells transfected with YFP-MR. Our imaging conditions thus result in primarily YFP peaks and include only a small, negligible contribution of autofluorescence. Untransfected $n = 7$, YFP-C10H-Ras $n = 15$ and YFP-MR $n = 37$. $* p < 0.05$; $** p < 0.01$; $*** p < 0.001$.

ular displacements (P_{cum}). For YFP-C10H-Ras, the size of the diffusing fraction is 27 %, 21 % and 18 % over increasing time lags (50, 100 and 150 ms respectively).

The resulting cumulative plot of molecular displacements (P_{cum}, dark grey line, Figure 4.3A) can be fitted with multiple population models. A one-population model failed to fit the curves well, while a two-population model did give an accurate fit (coarse dotted line, Figure 4.3A). Introduction of a third population hardly improved the fit and gave inconsistent results over different time lags (data not shown). We found that the mobility of membrane-associated YFP could be best described by two fractions each moving with a different speed: a large 'fast' fraction of 83 ± 2 % (Figure 4.3B), and a small 'slow' fraction of 17 ± 2 %. Subsequently, the mean squared displacements (MSDs) determined for both the fast and the slow fraction for each time lag were plotted as a function of the time lag (Figure 4.3C). For the fast fraction this resulted in a linear curve, indicating free diffusion of this fraction of molecules. Based on the slope of this curve a diffusion coefficient (D_{fast}) of 0.23 ± 0.01 mm^2/s was determined. The slow fraction, on the other hand showed displacements around our positional accuracy (0.0068 µm^2; indicated by triangle in Figure 4.3C). In previous studies, the mobility of the slow fraction of YFP-C10H-Ras was best described by confined diffusion, in which the molecules diffuse freely within a domain with impermeable borders (Lommerse et al., 2004; Schaaf et al., 2009). Different cell types showed large differences in the size of these restricted mem-

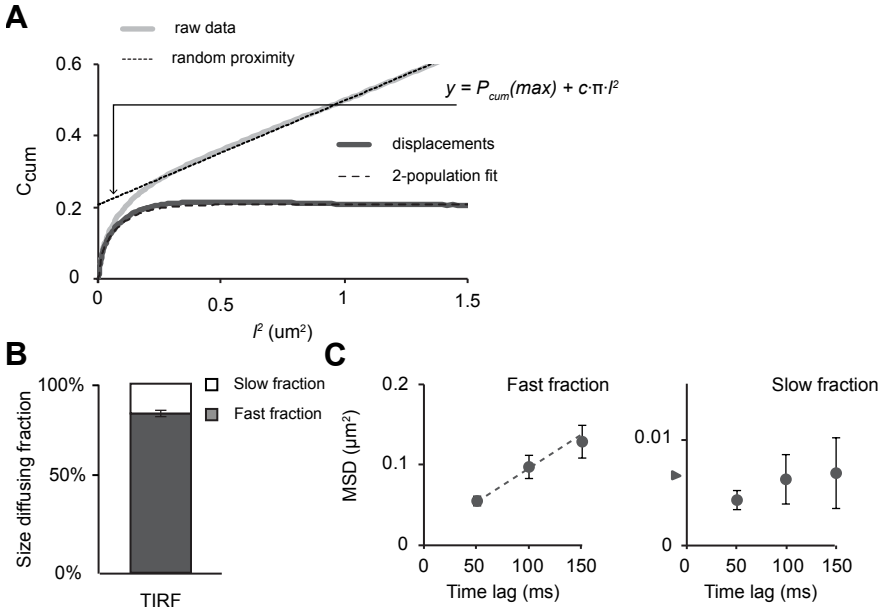

Figure 4.3: Proof of principle of TIRF microscopy using YFP-C10H-Ras
(A) PICS analysis. Shown is the cumulative plot of distances (l^2) for YFP-C10H-Ras with a time lag of 100 ms. The raw data (light grey line) contains contributions from both random proximity and molecule displacements. The contribution of distances due to random proximity can be fitted with a straight line (fine dotted line) and subtraction of these from the raw data leaves only the distances due to molecular displacement (dark grey line). The cumulative displacements are well fitted with a 2-population model of two moving fractions (coarse dotted line). (B-C) Quantification of diffusion of YFP-C10H-Ras. For YFP-C10H-Ras, 84 % of all molecules belong to the fast, freely diffusing fraction (B: grey bar, C: left panel). The remaining 16 % shows negligible displacement steps (B: white bar, C: right panel, positional accuracy indicated by the triangle) and are considered immobile. Data is shown as mean of recording days. $n = 3/17$ (days/cells).

		% slow	$D_{\mathbf{slow}}$(μm²/s)	**% fast**	$D_{\mathbf{fast}}$ (μm²/s)
YFP-C10H-Ras	TIRF	16 ± 2	n.a.	84 ± 2	0.23 ± 0.01
YFP-MR (CHO)	TIRF	51 ± 7	0.005 ± 0.001	49 ± 7	1.06 ± 0.48
	Wide-field	30 ± 2	0.031 ± 0.002	70 ± 2	1.45 ± 0.05
YFP-MR (COS-1)	TIRF	35 ± 6	0.015 ± 0.003	65 ± 6	0.36 ± 0.07
	Wide-field	11 ± 11	0.039 ± 0.018	89 ± 11	0.85 ± 0.17

Table 4.1: Comparison of single-molecule kinetics of YFP-C10H-Ras, YFP-YFP and YFP-MR between TIRFM and wide-field microscopy
% diffusing is the fraction of distances due to molecule displacements obtained from PICS analysis of the shortest time lag (50 ms).

brane domains. In the current study YFP-C10H-Ras does not show displacements larger than the spatial resolution, which suggest that in CHO cells this fraction represents either immobile molecules or molecules restricted to very small membrane domains (< 40 nm).

		Fraction of molecular displacements		
		50 ms	100 ms	150 ms
YFP-C10H-Ras	TIRF	27 %	21 %	18 %
YFP-MR (CHO)	TIRF	18 %	13 %	12 %
	Wide-field	12 %	12 %	13 %
YFP-MR (COS-1)	TIRF	14 %	13 %	12 %
	Wide-field	13 %	11 %	9 %

Table 4.2: Fraction of distances due to molecule displacement

Lower mobility of YFP-MR in TIRF than in wide-field microscopy suggestive for the existence of a membrane-associated population of YFP-MRs

Next, YFP-tagged human MR was examined. We chose to perform our experiments in CHO cells, since Grossmann et al. (2005, 2008) showed non-genomic, membrane-initiated signaling through the MR in these cells. In CHO cells, YFP-MR is seen throughout the cytoplasm in the absence of hormone and translocates to the nucleus upon stimulation with corticosterone (Figure 4.1C). When analyzed with conventional confocal microscopy, no obvious enrichment of YFP-MR at the membrane can be discerned (Figure 4.1C, insert).

We next imaged single-molecules of YFP-MR in CHO cells in TIRF and wide-field microscopy. In both TIRF and wide-field modus clear single YFP-MR molecules were observed. The molecular dynamics were analyzed using PICS, and the cumulative plot of observed peak distances was generated (C_{cum}; Figure 4.4A). We found that the fraction of measured distances as a result of molecular displacements of YFP-MR is larger in TIRF than in wide-field (for 50 ms: 18 % in TIRF and 12 % in wide-field; see also Table 4.2). Next, we fitted P_{cum} with a 2-population method and determined fraction sizes and MSDs of both fractions. In wide-field, a small fraction (30 ± 2 %) of YFP-MR showed small displacement steps. Plotting MSDs against the time lag resulted in a curve that could be fitted with a straight line, indicating free diffusion of this slow fraction. The diffusion coefficient (D_{slow}) was 0.031 ± 0.002 μm^2/s. The remaining 70 ± 2 % also showed free diffusion, but with ~50 fold larger displacements and a diffusion coefficient D_{fast} of 1.45 ± 0.05 μm^2/s (Figure 4.4B,C). Interestingly, when imaged in TIRF, the size of the slow fraction was larger: 51 ± 7 % (Figure 4.4B). At the same time, the displacements of both fractions were smaller (Figure 4.4C; $D_{\text{slow}} = 0.005 \pm 0.001$ μm^2/s; D_{fast} of 1.06 ± 0.48 μm^2/s).

To examine whether the observed difference in mobility patterns for YFP-MR between wide-field and TIRF imaging was specific for the cell line used, we repeated the same procedure in a second cell line, COS-1 cells. Also in COS-1 cells, conventional confocal microscopy failed to show an obvious enrichment of YFP-MR at the membrane (Figure 4.1D insert). Subsequently, YFP-MR expressing COS-1 cells were imaged using TIRF and wide-field single-molecule microscopy. The size of the

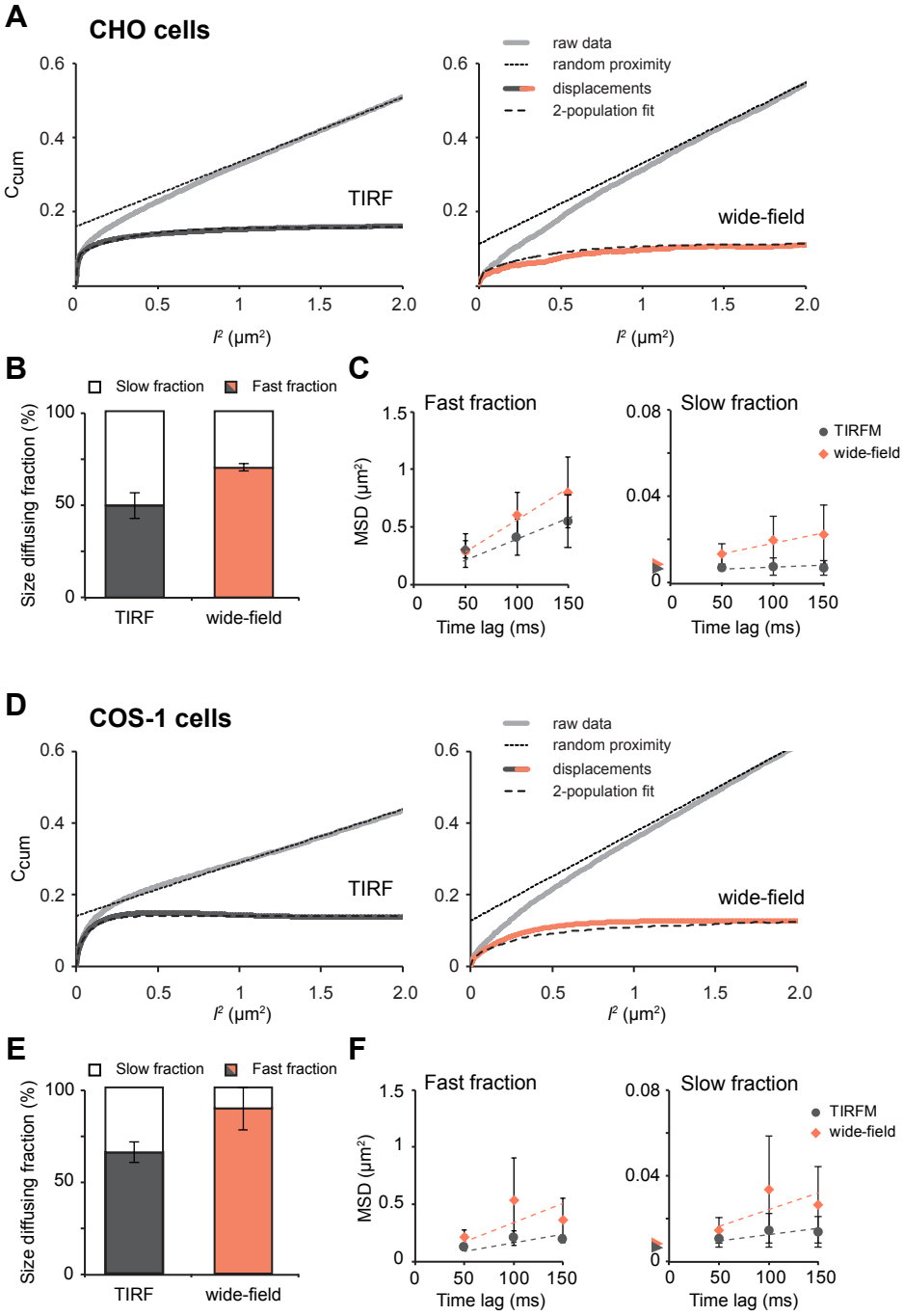
A
CHO cells
raw data
random proximity
displacements
2-population fit
TIRF
wide-field
Ccum
l² (μm²)
B
Slow fraction
Fast fraction
Size diffusing fraction (%)
TIRF
wide-field
C
Fast fraction
Slow fraction
TIRFM
wide-field
MSD (μm²)
Time lag (ms)
D
COS-1 cells
E
F

fraction of measured distances due to molecular displacements was highly similar between TIRF (14 %) and wide-field (13 %), see also Table 4.2. We found a larger slowly diffusing fraction in TIRF modus, highly comparable to what we observed in CHO cells. Only 11 ± 11 % of molecules showed slow diffusion in wide-field recordings, and in TIRF this fraction was increased to 35 ± 6 % (Figure 4.4E). In COS-1 cells, the measured diffusion coefficients of both the slow and the fast fraction were slightly decreased in TIRF (D_{fast} of 0.36 ± 0.07 μm^2/s versus 0.85 ± 0.17 μm^2/s in wide-field and D_{slow} of 0.015 ± 0.003 μm^2/s versus 0.039 ± 0.018 μm^2/s in wide-field; Figure 4.4F). In order to test for statistical significance we analyzed the diffusion patterns of YFP-MR separately for each recording day and tested significance for the full data set (CHO and COS-1 cells combined; $n =$ recording days). We found a significant difference between TIRF and wide-field recordings for the displacements of the slow fraction ($p = 0.04$) and for the size of the slow fraction ($p = 0.01$). No significant differences were seen between the two cell lines.

Corticosterone and BSA-bound corticosterone do not affect the mobility pattern of YFP-MR

In order to determine whether hormone treatment affects the kinetics of the receptor, a set of experiments was designed in which the receptor was exposed to its ligand. Ligand binding is known to alter the conformation of the receptor (at least in the cytoplasm) and to induce protein-protein interactions of membrane-associated steroid receptors (Levin, 2008). CHO cells were exposed to 1 μM corticosterone which is known to saturate MR binding (Karst et al., 2005), or to a similar concentration of BSA-conjugated corticosterone (cort-BSA). Cort-BSA is membrane-impermeable and any alteration in the kinetics of YFP-MR induced by this ligand will be the result of changes in the mobility of a membrane-associated YFP-MR. We assessed the mobility of YFP-MR by SMM before treatment and at 5 minutes after hormone treatment. The imaging took approximately 2 minutes, so diffusion was measured from 5–7 minutes post hormone treatment. We restricted ourselves to this short term treatment as it is known that membrane-associated receptors can become internalized by prolonged hormone treatment (Razandi et al., 2002; Wang and Wang, 2009; Karst et al., 2010). As a control, we tested the effects of the different hormone treatments on the kinetics of YFP-C10H-Ras.

Figure 4.4 *(preceding page)*: A smaller diffusing fraction of YFP-MR near the membrane in CHO and COS-1 cells
The diffusion behavior of YFP-MR recorded in TIRF and wide-field modes in both CHO (A-C) and COS-1 (D-F) cells. (A & D) Cumulative distances plots. (B & E) Fraction distributions. For both cell lines, the fraction of molecules that shows slow diffusion (white bars) is larger in TIRF than in wide-field. (C & F) MSD plots for both fractions (left panels: fast fractions, right panels: slow fractions). For CHO cells, the displacements of the slowly diffusing fraction are smaller in TIRF. Data is shown as mean of recording days. CHO: TIRF, $n = 5/45$; wide-field, $n = 4/43$; COS-1: TIRF, $n = 3/32$; wide-field, $n = 2/26$ (days/cells).

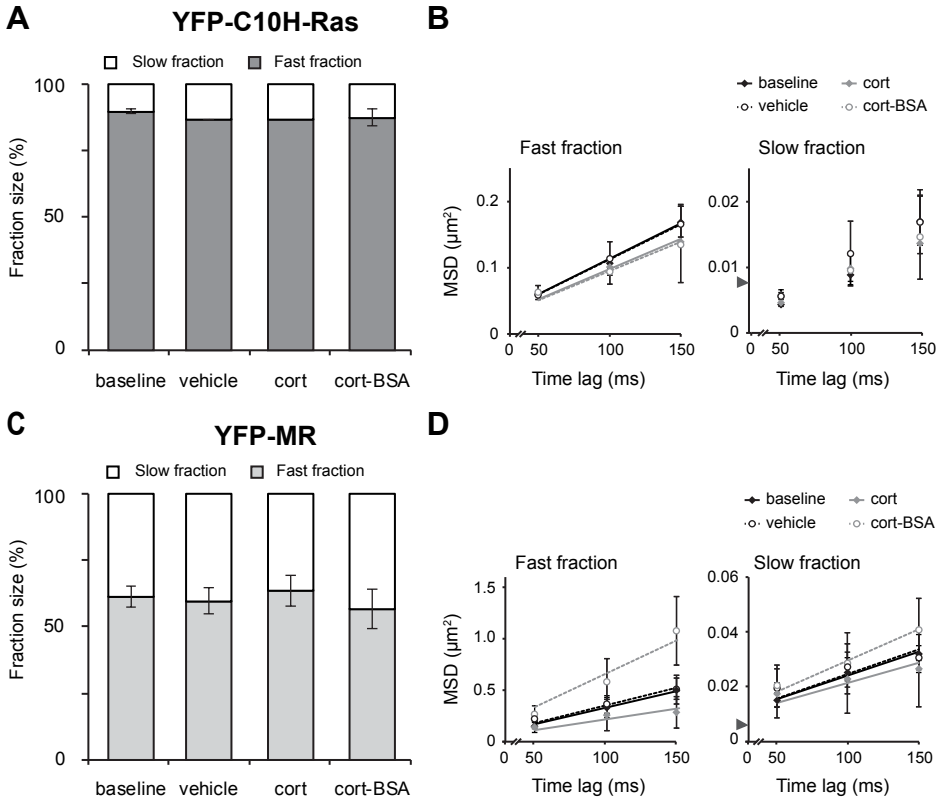

Figure 4.5: Corticosterone and cort-BSA do not affect diffusion behavior of YFP-C10H-Ras or YFP-MR

The effect of short-term treatment (5–7 min) with 100 nM corticosterone (cort) or BSA-conjugated corticosterone (cort-BSA) on fraction distribution was examined for both YFP-C10H-Ras (A-B) and YFP-MR (C-D). (A-B) Neither cort, cort-BSA, or vehicle treatment affected the fraction distribution (A) or the MSDs (B) of YFP-C10H-Ras, an inert membrane-associated molecule. (C-D) Hormone administration did not affect the fraction distribution (C) or the MSDs (D) of YFP-MR either. Data is shown as mean of recording days. YFP-C10H-Ras: baseline, $n = 4/18$; vehicle, $n = 3/7$; cort, $n = 2/5$; cort-BSA, $n = 2/6$. YFP-MR: baseline, $n = 6/64$; vehicle, $n = 5/18$; cort, $n = 4/21$; cort-BSA, $n = 4/25$ (days/cells).

		% slow	D_{slow} ($\mu m^2/s$)	**% fast**	D_{fast} ($\mu m^2/s$)
YFP-C10H-Ras	Baseline	10 ± 1	n.a.	90 ± 1	0.28 ± 0.01
	Vehicle	13 ± 0	n.a.	87 ± 0	0.27 ± 0.00
	Cort	13	n.a.	87	0.23
	Cort-BSA	13 ± 3	n.a.	87 ± 3	0.29 ± 0.01
YFP-MR	Baseline	39 ± 4	0.04 ± 0.00	61 ± 4	0.77 ± 0.03
	Vehicle	40 ± 5	0.05 ± 0.01	60 ± 5	1.00 ± 0.07
	Cort	36 ± 6	0.04 ± 0.01	64 ± 6	0.58 ± 0.07
	Cort-BSA	43 ± 8	0.06 ± 0.00	57 ± 8	1.46 ± 0.14

Table 4.3: Effect of hormone treatments on protein kinetics of YFP-C10H-Ras and YFP-MR in CHO cells

Treatment with vehicle, corticosterone or cort-BSA did not change the displacements nor the relative fraction sizes of YFP-C10H-Ras (Figure 4.5A–B; Table 4.3). Next, we subjected the same treatments to YFP-MR-transfected CHO cells. However, no effects were seen with either treatment. Thus, the slowly diffusing fraction of YFP-MR (measured using TIRF microscopy) remains around 40 % with either treatment (Figure 4.5C). MSDs and diffusion coefficients were not affected by hormone treatment either (Figure 4.5D; Table 4.3).

4.4 Discussion

In the present study we have investigated YFP-tagged MR using single-molecule microscopy in TIRF and wide-field mode. The results are summarized in Tables 4.1 till 4.3. TIRF is a well-established method that provides images that are strongly enriched for near-membrane molecules (Axelrod, 2008). Thus, if a membrane-associated subpopulation of YFP-MR was present in the investigated cell lines, it would have been be strongly enriched for in TIRF. We analyzed the protein dynamics of YFP-MR with SMM in wide-field and TIRF in two cell lines, and observed a larger slow fraction of YFP-MR molecules in TIRF versus wide-field modes in both cell lines (51 % versus 30 % and 35 % versus 11 %, see Table 4.1). In one cell line (CHO), the slow fraction also showed slower diffusion in TIRF as compared to wide-field microscopy.

In general, membrane-associated proteins are less mobile than cytoplasmic proteins (Owen et al., 2009; Sanderson, 2012), mainly due to the higher viscosity of the membrane. Diffusion of membrane-anchored proteins ranges from 0.01 to 1.0 $\mu m^2/s$ (Owen et al., 2009). The diffusion of the observed slow fraction of YFP-MR (D_{slow} of 0.012 and 0.015 $\mu m^2/s$ in CHO and COS-1 cells respectively) fits within this expected range for membrane-anchored proteins. Cytoplasmic MR, in contrast, is expected to diffuse much faster. The diffusion of steroid receptors has never been analyzed within the cytoplasm, but has extensively been measured in the nucleus. We found that both the MR and GR diffuse with a diffusion coefficient of 2–3 $\mu m^2/s$ (*Chapters 5 and 6*) within the nucleus, and similar diffusion would be expected for the cytoplasmic fraction. Here, we obtained a fast diffusing fraction with D_{fast} of 1.4 and 0.9 $\mu m^2/s$ (in CHO and COS-1 cells respectively), which is slightly lower than expected for freely diffusing cytoplasmic MR. The MR is bound by a large chaperone complex within the cytoplasm (Picard, 2006), which could underlie this slower diffusion. Taken together, the slow fraction shows diffusion that fits to what is known for membrane-associated proteins and the fast fraction diffuses slightly slower than what is expected for cytoplasmic steroid receptors.

Of note, we did find a slowly diffusing fraction of 11–30 % in wide-field recordings where we expect a negligible contribution of the membrane-associated population. This suggests that also cytoplasmic MR encompasses a slowly diffusing frac-

tion (potentially due to protein complex formation) and we thus do not presume that the entire slow fraction will represent membrane-associated MR. The larger size of the slowly diffusing fraction measured using TIRF microscopy fits very well with the notion of a mixed cytoplasmic (both fast and slow diffusing populations) and membrane-associated (purely slow diffusing) population of the MR in TIRF.

There is one large difference between TIRF and wide-field recordings that could influence the obtained protein diffusion: the thickness of the optical slice (or Z-depth). By default, the Z-depth of TIRF is very small and estimated to be around 60–100 nm thick. In contrast, our wide-field recordings will have a Z-depth of 0.5–1 µm (van Royen et al., 2014). As proteins diffuse in 3D, they will 'escape' from the field of view during the time lag. This effect will be larger when a smaller Z-depth is used (as in TIRF) and will occur most readily for fast diffusing molecules (van Royen et al., 2014). Thus, a smaller Z-depth will enrich for slowly moving molecules and the larger size of the slow fraction observed using TIRF could therefore represent an artifact of the imaging conditions. However, the results from our PICS analysis show that in TIRF mode fewer molecules 'escape' than in wide-field mode. With PICS analysis we could directly calculate the fraction of recorded distances that are due to molecule displacements from the C_{cum} graphs (Figure 4.3C). When this fraction is large, many molecules are imaged in two consecutive images, so only few molecules leave the z-plane during the interval between the images. We found that a similar or even larger fraction of molecules can be imaged in two consecutive images in TIRF mode (Table 4.2). In CHO cells, for example, 18 % of molecules can be imaged in two consecutive images, while this drops to 12 % in wide-field recordings. Thus, even though the z-depth is a lot smaller in TIRF mode, more molecules are imaged in two consecutive images, indicating that fewer molecules 'escape' from the z-slice. We therefore conclude that there is a true enrichment for slowly diffusing YFP-MRs near the membrane in TIRF mode, and that the increased size of the slow fraction observed in TIRF recordings of YFP-MR is not an artifact of the imaging conditions.

Conclusively, we find a larger fraction of slowly diffusing molecules for YFP-MR in TIRF as compared to wide-field microscopy, and this difference cannot be accounted for by technical artifacts. The most likely explanation for the increased size of this fraction in TIRF would be the enrichment for membrane-associated proteins in TIRF that show slower diffusion. Alternatively, the slower diffusion near the membrane may not result from association with the membrane, but may be due to steric hindrance or a higher concentration of signaling partners in the cytoplasmic region near the membrane.

Manipulation of the membrane-associated fraction

In the current study we applied corticosterone or its membrane-impermeable conjugate cort-BSA to YFP-MR expressing cells. Unfortunately, we did not find any effect of either hormone on the dynamics of YFP-MR in TIRF (Table 4.3), indicating

that the mobility of a putatively membrane-associated MR population is not altered upon ligand binding. It has been reported for many membrane receptors that ligand activation affects protein mobility within our time range. For example, treatment with insulin led to rapid (within 5 minute) recruitment of H-Ras to smaller microdomains (Lommerse et al., 2005). In another study, the chemotactic receptor cAR1 was activated by its ligand cAMP. This resulted, within a minute, into a larger diffusing fraction (Keijzer et al., 2008). On the other hand, ligand treatment does not necessarily affect protein dynamics. The available literature suggests that a membrane-associated MR will bind adaptor proteins upon activation, but is also bound to other proteins (such as caveolin-1) before activation (Grossmann et al., 2010; Pojoga et al., 2010b), which could result in no net change in diffusional characteristics after activation.

Other options remain to specifically alter the dynamics of the membrane-associated MR population. Disruption of lipid rafts, caveolae or actin compartmentalization are all known to affect the kinetics of membrane-associated proteins (Lajoie et al., 2007; Ganguly et al., 2008). Moreover, as the MR is presumably also localized in caveolae (Pojoga et al., 2010b) and is known to associate with lipid rafts (Grossmann et al., 2010), disruption of these structures would likely affect the membrane-association of the MR as well. Future studies that specifically disrupt the membrane-associated fraction of the MR would provide the final proof that TIRF can enrich for this population in a sufficient manner to distinguish it from the cytoplasmic background.